

# Lifting 2D Object Locations to 3D by Discounting LiDAR Outliers across Objects and Views

Robert McCraith<sup>1</sup>, Eldar Insafutdinov<sup>2</sup>, Lukas Neumann<sup>3</sup>, Andrea Vedaldi<sup>4</sup>

**Abstract**—We present a system for automatic converting of 2D mask object predictions and raw LiDAR point clouds into full 3D bounding boxes of objects. Because the LiDAR point clouds are partial, directly fitting bounding boxes to the point clouds is meaningless. Instead, we suggest that obtaining good results requires sharing information between *all* objects in the dataset jointly, over multiple frames. We then make three improvements to the baseline. First, we address ambiguities in predicting the object rotations via direct optimization in this space while still backpropagating rotation prediction through the model. Second, we explicitly model outliers and task the network with learning their typical patterns, thus better discounting them. Third, we enforce temporal consistency when video data is available. With these contributions, our method significantly outperforms previous work despite the fact that those methods use significantly more complex pipelines, 3D models and additional human-annotated external sources of prior information.

## I. INTRODUCTION

Robotics applications often require to recover the 3D shape and location of objects in world coordinates. This explains the proliferation of datasets such as KITTI, nuScenes and SUN RGB-D [7], [2], [34] which allow to train models that can classify, detect and reconstruct objects in 3D from sensors such as cameras and LiDARs. However, creating such datasets is very expensive. For example, [32], [39] report that manually annotating a single object with a 3D bounding box requires approximately 100 seconds. While this cost has since been reduced [19], it remains a significant bottleneck in data collection.

In some cases, cross-modal learning can substitute manual annotations. An example is monocular depth prediction, where supervision from a LiDAR sensor is generally sufficient [6]. Unfortunately, this does not extend to tasks such as object detection. For instance, a dataset such as KITTI provides only 7481 video frames annotated with objects due to the cost of manual annotation.

In this work, we thus consider the problem of detecting objects in 3D, thus also automatically annotating them in 3D, but using only standard 2D object detector trained on a generic dataset such as MS-COCO [15], which is disjoint from the task-specific dataset (in our case KITTI for 3D car detection). We assume to have as input a collection of video frames, the corresponding LiDAR readings from the viewpoint of a moving vehicle, and the ego-motion of the vehicle. We also assume to have a pre-trained 2D detector and

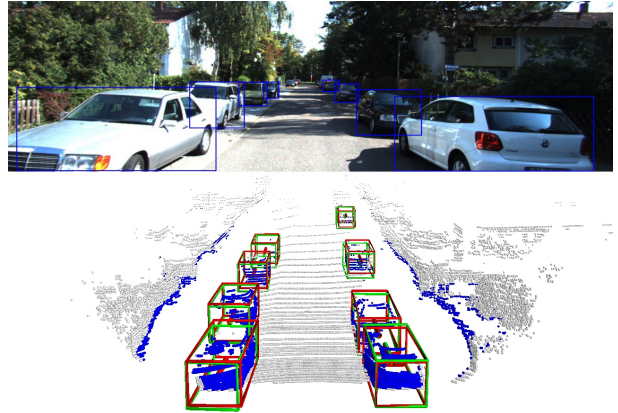


Fig. 1: Our Method (green) vs KITTI label (red), no Ground Truth is used to train our model.

segmenter such as Mask R-CNN for the objects of interest (e.g., cars). With this information, we wish to train a model which takes in raw LiDAR point cloud and outputs full 3D bounding box annotation for the detected objects without incurring any further manual annotation cost.

There are three main challenges. First, due to self and mutual occlusions, the LiDAR point clouds only cover part of the objects in a context dependent manner. Second, the LiDAR readings are noisy, for example sometimes seeing through glass surfaces (windows) and sometimes not. Third, the available 2D segmentations may not be perfectly semantically aligned with the target class (e.g., ‘vehicles’ vs ‘cars’), are affected by a domain shift, and may not be perfectly geometrically with the LiDAR data, resulting in a large number of outlier 3D points arising from background objects.

We propose an approach based on the following key ideas. First, because the LiDAR point cloud can only cover the object partially, it is impossible to estimate the full 3D extent of the object from a single observation of it. Instead, we share information between all predicted 3D boxes in the dataset by *learning a 3D bounding box predictor from all the available data*. We further aid the process by injecting weak prior information in the form of a single fixed 3D mesh template of the object (an ‘average car’), but avoid sophisticated 3D priors employed in prior works [44], [29].

We then introduce three improvements to the ‘obvious’ baseline implementation of this idea. First, we show that a key challenge in obtaining good 3D bounding boxes is to estimate correctly the yaw (rotation) of the object. This is particularly challenging for partial point clouds as several ambiguous fits (generally up to rotations of 90 degrees) often exist. Prior work has addressed this problem by using pre-

<sup>1,2,4</sup> Authors are with Visual Geometry Group, Dept. of Engineering Science, University of Oxford, <sup>3</sup> Lukas is with Faculty of Electrical Engineering, Czech Technical University in Prague. {robert, eldar, lukas, vedaldi}@robots.ox.ac.uk

trained yaw predictors, requiring manual annotation. Here, we learn the predictor automatically from the available data only. To this end, we show that mere local optimization via gradient descent works poorly; instead, we propose to systematically explore a full range of possible rotations for each prediction, backpropagating the best choice every time. We show that this selection process is very effective at escaping local optima and results in excellent, and automated, yaw prediction.

Second, we note that the LiDAR data contains significant outliers. We thus propose to automatically learn the *pattern* of such outliers by predicting a confidence score for each 3D point, treated as a Gaussian observation. These confidences are self-calibrated using a neural network similar to the ones used for point cloud segmentation, configured to model the aleatoric uncertainty of the predictor.

Third, we note that we generally have at our disposal *video data*, which contains significant more information than instantaneous observations. We leverage this information by enforcing a simple form of temporal consistency across several frames.

As a result of these contributions we obtain a very effective system for automatically labelling 3D objects. Our system is shown empirically to outperform relevant prior work by a large margin, all the while being simpler, because it uses less sources of supervision and because it does *not* use sophisticated prior models of the 3D objects nor a large number of 3D models as priors [44], [29]

## II. RELATED WORK

**a) Supervised:** 3D object detection methods assume availability of either monocular RGB images, LiDAR point clouds or both. Here we focus on supervised methods using 3D point cloud inputs. [37], [4] discretise point clouds onto a sparse 3D feature grid and apply convolutions while excluding empty cells. [3] project the point cloud onto the frontal and the top views, apply 2D convolutions thereafter and generate 3D proposals with an RPN [30]. [46] convert the input point cloud into a voxel feature grid, apply a PointNet [28] to each cell and subsequently process it with a 3D fully convolutional network with an RPN head which generates object detections. Frustum PointNets [27] is a two step detector which first detects 2D bounding boxes using these to determine LiDAR points of interest which are filtered further by a segmentation network. The remaining points are then used to infer the 3D box parameters with the centre prediction being simplified by some intermediate transformations in point cloud origins. We are using Frustum PointNets as a backbone for our method.

**b) Weakly Supervised:** Owing to the complexity of acquiring a large scale annotated dataset for 3D object detection many works recently have attempted to solve this problem with less supervision. [19] the required supervision is reduced from the typical  $(X, Y, Z)$  centre,  $yaw$ ,  $(x_1, y_1, x_2, y_2)$  2D box and  $(l, w, h)$  3D size they instead annotate 500 frames with centre  $(X, Z)$  in the Birds Eye View and finely annotating a 534 car subset of these frames to achieve accuracy similar to models trained on the entire Kitti training set. This however can result in examples in the larger

training set or validation set which are outside the distribution of cars seen in the smaller subset, are also susceptible to the problems mentioned in [5] and the weakly annotated centres can have a large difference to the Kitti annotations. In [44] trains DeepSDF[22] on models from a synthetic dataset which are then rendered into the image and iteratively refined to produce a prediction that best fits the predictions of Mask R-CNN outputs. This however takes 6 seconds to refine predictions on each input example and ground truth 2D boxes are used to select cars used to train on. In [29] 3D anchors densely placed across the range of annotations are projected into the image with object proposed by looking at the density of points within or nearby the anchors in 3D and the 3D pose and 2D detections are supervised by a CNN trained on Beyond PASCAL[41]. In [13] instance segmentation is used to place a mesh in the location of detected cars which is refined using supervised depth estimation.

**c) Viewpoint estimation:** Estimating 3D camera orientation is an actively researched topic [25], [12], [36], [33], [20], [26], [14]. Central to this problem is the choice of an appropriate representation for rotations. Directly representing rotations as angles  $\theta \in [0, 2\pi)$  suffers from discontinuity at  $2\pi$ . One way to mitigate this is to use the trigonometric representation  $(\cos \theta, \sin \theta)$  [24], [17], [1]. Another approach is to discretise the angle into  $n$  quantised bins and treat viewpoint prediction as a classification problem [36], [33], [20]. Quaternions are another popular representation of rotations used with neural networks [12], [43]. Learning camera pose without direct supervision, for example, when fitting a 3D model to 2D observations, may suffer from ambiguities due to the object symmetries [31]. Practically, this means that the network can get stuck in a local optima of  $SO(3)$  space and not be able to recover the correct orientation. Several recent works [35], [10], [8] overcome this by maintaining several diverse candidates for the estimated camera rotation and selecting the one that yields the best reconstruction loss. Our approach discussed in sec. III-C is most related to these methods.

## III. METHOD

Our goal is to estimate the 3D bounding box of objects given as input videos with 2D mask predictions and LiDAR point clouds. We discuss first how this problem can be approached by direct fitting and then develop a much better learning-based solution.

### A. Shape model fitting

We first describe how a 3D bounding box can be fitted to the available data in a direct manner. To this end, let  $I \in \mathbb{R}^{3 \times H \times W}$  be a RGB image obtained from the camera sensor and let  $L \subset \mathbb{R}^3$  be a corresponding finite collection of 3D points  $\mathbf{X} \in L$  extracted from the LiDAR sensor. Furthermore, let  $m \in \{0, 1\}^{H \times W}$  be the 2D mask of the object obtained from a system such as Mask R-CNN [9] from image  $I$ . Our goal is to convert the 2D mask  $m$  into a corresponding 3D bounding box  $B$ .

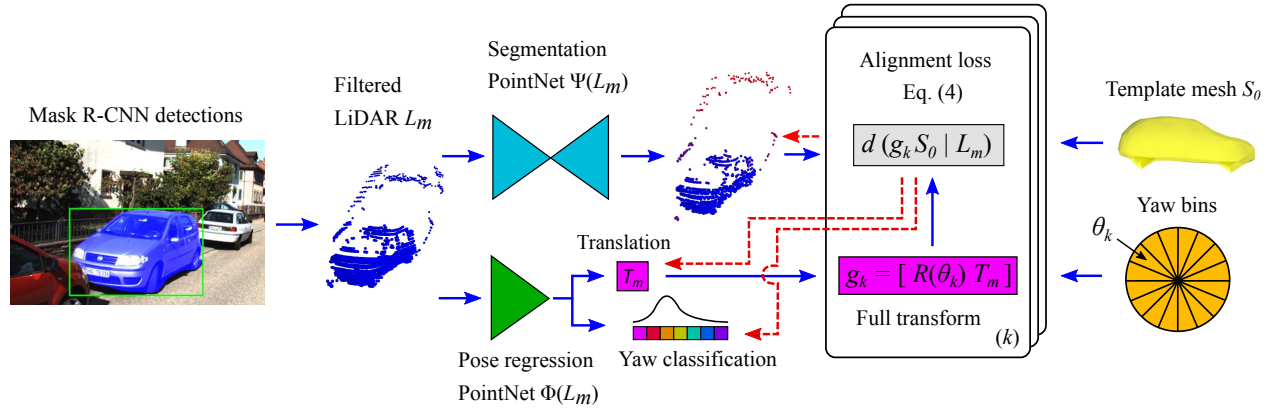


Fig. 2: Network architecture. Dashed arrows in red show the flow of the gradients during the backward pass. Alignment loss is evaluated for each yaw bin  $\theta_k$  and the optimal yaw is used to supervise the yaw classification network  $\Phi_r$  (see sec. III-C).

To do so, assume that the LiDAR points are expressed in the reference frame of the camera and that the camera calibration function  $k: \mathbb{R}^2 \rightarrow \Omega = \{1, \dots, H\} \times \{1, \dots, W\}$  is known. The calibration function is defined such that the 3D point  $\mathbf{X} = (X, Y, Z)$  projects onto the image pixel  $u = k(\pi(\mathbf{X}))$  where  $\pi(X, Y, Z) = (X/Z, Y/Z)$  is the perspective projection. In particular, the subset of LiDAR points  $L_m \subset L$  that project onto the 2D mask  $m$  is given by:  $L_m = L \cap (k \circ \pi)^*(m)$  where  $*$  denotes the pre-image of a function. In practice, this is a crude filtering step, because the masks are imprecise and not perfectly aligned to the LiDAR and because LiDAR may sometimes see ‘through’ the object, for instance in correspondence of glass surfaces (see Fig. 3).

In order to fit a 3D bounding box  $B$  to  $L_m$ , we use a weak prior on the 3D shape of the object. Specifically, we assume that a 3D template surface  $S_0 \subset \mathbb{R}^3$  is available, for example as simplicial (triangulated) mesh. We fit the 3D surface to the LiDAR points by considering a rigid motion  $g \in SE(3)$  which, applied to  $S_0$ , results in the posed mesh  $S = gS_0 = \{g\mathbf{X} : \mathbf{X} \in S_0\}$ . We then define a distance between the mesh and the 3D LiDAR points as follows:

$$d(S|L_m) = \frac{1}{|L_m|} \sum_{\mathbf{X} \in L_m} \min_{\mathbf{X}' \in S} \|\mathbf{X}' - \mathbf{X}\|^2. \quad (1)$$

This quantity is similar to a Chamfer distance, but it only considers half of it: this is because most of the 3D points that



Fig. 3: For each pair, left: RGB input image with Mask R-CNN predicted box and highlighted pixels inside the mask. Right: LiDAR points in blue represent those inside the 2D mask, green those outside. Note that, while the image mask removes many outliers, many remain at the object boundaries and transparent surfaces.

belong to the template object are *not* be visible in a given view (in particular, at least half are self-occluded), so not all points in the template mesh have a corresponding LiDAR point.

Given a 2D object mask  $m$  and its corresponding LiDAR points  $L_m$ , we can find the pose  $g$  of the object by minimizing  $d(gS_0|L_m)$  with respect to  $g \in SE(3)$ . Then the bounding box of the object  $m$  is given by  $gB_0$  where  $B_0 \subset \mathbb{R}^3$  is the 3D bounding box that tightly encloses the template  $S_0$ .

In accordance with prior work [7], [29], [19], we can in practice carry out the minimization not over the of full space  $SE(3)$ , but only on 4-DoF transformation  $g = [R_\theta, \mathbf{T}]$  where the rotation  $R_\theta$  is restricted to the yaw  $\theta$  (rotation perpendicular to the ground plane). Even so, direct minimization of (1) is in practice prone to failure because individual partial LiDAR point clouds do not contain sufficient information and fitting results are thus ambiguous (we do not report results in this setting as they are extremely poor).

Our solution to the ambiguity of fitting (1) is to *share information* across all object instances in the dataset. We do this by training a deep neural network  $\Phi: \text{Fin}(\mathbb{R}^3) \rightarrow SE(3)$  mapping the LiDAR points  $L_m$  to the corresponding object pose  $g = \Phi(L_m)$  directly. The network  $\Phi$  can be trained in a self-supervised manner by minimizing (1) averaged over the entire dataset  $\mathcal{D}$  as

$$\mathcal{L}(\Phi|\mathcal{D}) = \frac{1}{|\mathcal{D}|} \sum_{(L_m, m) \in \mathcal{D}} d(g_m S_0 | L_m) \quad (2)$$

where  $g_m = \Phi(L_m)$ .

### B. Modelling and discounting outliers

A major drawback of (2) is that LiDAR points tend to be noisy, especially because the boundaries of the region  $m$  may not correspond to the object exactly or the LiDAR may be affected by a reflection or ‘see through’ a glass surface. Such points might disproportionately skew the loss term, forcing the estimated object position closer to these outliers. In order to help the model discriminate between inliers and outliers, we let the network predict an estimate of whether a given measurement is likely to belong to the object or not.



Fig. 4: Even after removing LiDAR points which do not project into the 2D instance mask we still have a large number of outliers, mainly caused by partial occlusions and points at the boundary where 2D masks struggle. The  $\sigma^2(\mathbf{X})$  value predicts the relevance of a point to the cars location with blue points having low values with a gradient to red for higher values which suggests the point is an outlier.

We therefore propose a second network  $\sigma(\mathbf{X}) = \Psi_{\mathbf{X}}(L_m)$  that assigns to each LiDAR point  $\mathbf{X} \in L_m$  a variance  $\sigma$  and jointly optimize  $\Phi$  and  $\Psi$  by minimizing [21], [11]:

$$\bar{d}(S|L_m) = \frac{1}{|L_m|} \sum_{\mathbf{X} \in L_m} \min_{\mathbf{X}' \in \hat{S}} \frac{\|\mathbf{X}' - \mathbf{X}\|^2}{\sigma^2(\mathbf{X})} + \log \sigma^2(\mathbf{X}) \quad (3)$$

Note that the network  $\Psi$  has to make a judgement call for every point  $\mathbf{X}$  on whether it is likely to be an outlier or not *without* having access to the loss. A perfect prediction (i.e., one that minimizes the loss) would set  $\sigma(\mathbf{X}) = \|\mathbf{X}' - \mathbf{X}\|$  to be the same as the fitting error. The desirable side effect is that, in this manner, outliers are discounted by a large  $\sigma(\mathbf{X})$  when it comes to estimating the pose  $g_m$  of the object.

### C. Direct optimization for the yaw

Finally, we note that fitting the rotation of the object can be ambiguous, especially if only a small fragment of the object is visible in the RGB/LiDAR data. Specifically, the distance  $\bar{d}([R_{\theta_m} \mathbf{T}_m]S_0|L_m)$ , which is usually well behaved for the translation component  $\mathbf{T}_m$ , has instead a number of ‘deep’ local minima, which we found is mainly caused by the inherent ambiguities of fitting the rotation  $\theta_m$  (yaw) parameter. Each minimum corresponds to a  $90^\circ$  rotation as in many example only a single side of the vehicle is visible. In practice, as we show, the yaw network  $\Psi$  *can* learn to disambiguate the prediction, but it usually fails to converge to such a desirable solution without changes in the formulation.

In order to solve this issue, we propose to modify the formulation to incorporate *direct optimisation* over the yaw. In other words, every time the loss is evaluated, we assess a number of possible rotations  $R$ , as follows:

$$R_m^* = \operatorname{argmin}_{R \in \mathcal{R}} \bar{d}([R \mathbf{T}_m]S_0|L_m) \quad (4)$$

$$\bar{r} = \|R_m - R_m^*\| \quad (5)$$

$$\mathcal{L}'(\Phi, \Psi|\mathcal{D}) = \frac{1}{|\mathcal{D}|} \sum_{(L_m, m) \in \mathcal{D}} \bar{d}([R_m^* \mathbf{T}_m]S_0|L_m) + \bar{r} \quad (6)$$

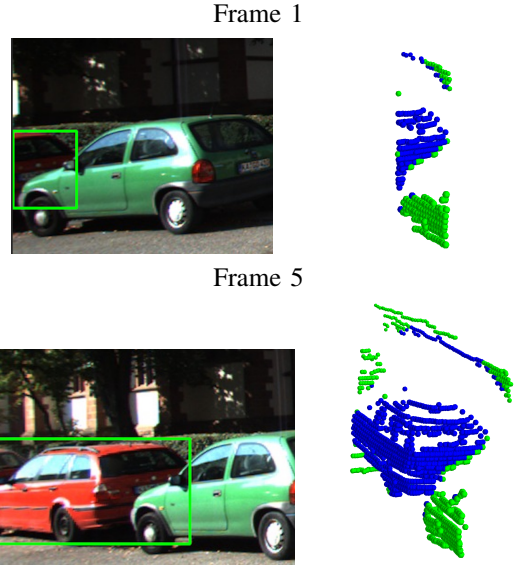


Fig. 5: Two frames in a sequence of five, with a heavily occluded and truncated car in the first frame and a much better view of the same in the last. Multi-frame consistency allows the method to use clearer frames to interpret more difficult ones, which is particularly helpful in discovering the outliers.

The loss is the same as before for the translation, but, given the predicted translation, it always explores all possible rotations  $R$ , picking the best one  $R_m^*$ .

Note that this does not mean that the network  $\Phi$  is not tasked with predicting a rotation anymore; on the contrary, the network is encouraged to output the optimal  $R_m^*$  via minimization of the term  $\|R_m - R_m^*\|$ . This has the obvious benefit of not incurring the search at test time, and therefore the final network running time is not affected by this process.

In practice, as only the yaw angle is predicted, we implement this loss by quantizing the interval  $[0, 2\pi)$  in 64 distinct values (bins), as in our experiments we found this number of bins sufficient (see results in table II). In this manner, the rotation head of the network  $\Phi$  can be interpreted as a softmax distribution  $\Phi_r(L_m)$  and the norm  $\|\cdot\|$  is replaced by the cross-entropy loss.

### D. Multi-frame consistency

Whilst in our approach we do not have the actual 3D pose of the object available as a training signal, the 3D pose of the object across multiple frames must be consistent with the observer ego-motion. This is true for vehicles that are not moving (parked cars) and approximately true for other vehicles; in particular, the *yaw* of the objects, once ego-motion has been compensated for, is roughly constant.

Specifically, consider an arbitrary model point  $\mathbf{X}_0 \in S_0$ . Observed in a LiDAR frame  $i$ , this point is estimated to be at location  $\mathbf{X}_0^i = g^i \mathbf{X}_0$ , where  $g^i$  is the network prediction for frame  $i$ . Likewise, let  $\mathbf{X}_0^j = g^j \mathbf{X}_0$  be the point position at frame  $j$ . If the object is at rest, the two positions are related by  $\mathbf{X}_0^i = g_{i \leftarrow j} \mathbf{X}_0^j$  where  $g_{i \leftarrow j}$  is the ego-motion between frames  $i$  and  $j$  of the vehicle where the sensors are mounted, which



we assume to be known. We can thus define the consistency loss  $\mathcal{L}^{\mathbf{X}_0}$  for any model point  $\mathbf{X}_0$ :

$$\mathcal{L}^{\mathbf{X}_0}(\Phi|\mathcal{D}) = \frac{1}{|\mathcal{D}|} \sum_{i=1}^N \sum_{(L_m, m) \in \mathcal{D}^i} \sum_{j=1}^K \|g_{i \leftarrow i+j} \mathbf{X}_0^{i+j} - \mathbf{X}_0^i\|^2. \quad (7)$$

where  $\mathcal{D}^i$  denotes LiDAR-mask pairs detected in the frame  $i$ ,  $K$  is the length of the frame sequence over which the consistency is evaluated, and  $N$  is the total number of frames.

Note that loss (7) is null for all object keypoints if, and only if,  $g^i = g_{i \leftarrow j} g^j$ , which is an *equivariance* condition for the predictor. However, we found it more convenient and robust to enforce this equivariance by using (7) summed over a small set of representative model points. In our experiments we have found that at least two points are required to ensure that we consistently predict the heading (yaw) of the detected car. In practice, we use car centre and front keypoints (see Fig. 6), so the final loss term used to train the model is:

$$\mathcal{L}(\Phi, \Psi|\mathcal{D}) = \mathcal{L}'(\Phi, \Psi|\mathcal{D}) + \mathcal{L}^{\mathbf{X}_{\text{centre}}}(\Phi|\mathcal{D}) + \mathcal{L}^{\mathbf{X}_{\text{front}}}(\Phi|\mathcal{D}) \quad (8)$$

**a) Implementation details of tracking:** A detector such as Mask R-CNN only provides 2D mask for individual video frames, but defining the loss (7) requires to identify or track the same object across two frames. For tracking, we take the median of LiDAR points for each mask and compare them to the medians of masks in adjacent frames. The closest pseudo-centres are chosen to be the same vehicle if and only if the number of LiDAR points has not changed significantly and the distance between them is less than 2 meters when ego motion is accounted for. The distance criterion ensures that the same vehicle is detected while the number of points removes poor Mask-RCNN detections in subsequent frames. This tracking is only used at training time, at test time we use all 2D detections.

#### IV. EXPERIMENTS

We assess our methods against the relevant state of the art on standard benchmarks.

**a) Data:** For our experiments, we use the KITTI Object Detection dataset [7] which has 7481 frames with labels in 3D.

However, we do so for compatibility with prior work. Specifically, we use the split found in [3], the standard across all prior works which first splits the videos into training and validation sets focusing on two different parts of the world (no visual overlap). The network is learned on the training videos using multiple frames and then applied and evaluated on the validation videos on a single-frame basis.

KITTI evaluates vehicle detectors using Birds Eye View (BEV) IOU and 3D box IOU (3D) with a strict cutoff of 0.7 for a positive detection. To be compatible with other relevant works in automated labelling [44], [29], we evaluate instead at a threshold of 0.5, also used for other KITTI categories, which reduces the influence of object size on IoU performance. In part, this is motivated by [5] which notes that the size of the ‘ground-truth’ KITTI annotations are often imprecise due

to the fact that many object instances have few LiDAR points and thus it is difficult for human annotators to accurately estimate metric size.

**b) Data preprocessing:** To construct our training set we first run Mask-RCNN [9], [40] with the ResNet 101 backend to locate cars in the images. We then extract the LiDAR points contained within the masks detected and use these for 3D labelling. When tracking for 5 frames this gives us 9.6k cars in the training. For evaluation we only use a single frame of Mask R-CNN detection and use the mask score as the confidence for our predictions.

**c) Implementation:** We implement our method in Pytorch [23] and use components from Frustum PointNets [27] to construct our network. All variants are trained with Adam optimizer with a learning rate of  $3 \times 10^{-3}$  decreasing every 30 steps with multiplier 0.3 for a total of 150 epochs with a batch size of 64. Training was performed on a single Titan RTX with a Ryzen 3900X processor and the most complex models had a training time of 7 hours.

##### A. Ablations of model components

We first start by analysing the individual components of our model (table I). First, we do not use the 2D mask to filter LiDAR points, significantly increasing the number of outliers, arising in particular from cars proximal to the target one (row (a)).

Masking LiDAR points (row (b)) results in a substantial improvement, removing most of these outliers (see also Fig. 3). Introducing the temporal consistency/equivariance loss (7) (row (c)) does not give by itself a noticeable benefit because outlier points are still heavily influential to the prediction. Discounting outliers using the probabilistic formulation of (3) increases accuracy substantially (row (d)). Furthermore, bringing back the consistency loss, which amounts to our full model, does now show a significant benefit (row (e)). Our interpretation is that considering multiple frames can significantly aid discovering and learning outlier patterns: this is because outliers tend to be *inconsistent* across frames, so reasoning over multiple frames helps discovering them (see Fig. 5).

TABLE I: Ablation of different components of the model and data processing steps. Our full model with automatic outlier discounting and multi-view consistency achieves the highest accuracy.

	Filtering	Components		AP <sub>BEV</sub> (IoU = 0.5)		
		Outlier-aware	Multi-view	Easy	Moderate	Hard
(a)	2D Box			35.53	41.54	33.96
(b)	2D Mask			58.61	62.56	54.20
(c)	2D Mask		✓	58.63	61.70	54.11
(d)	2D Mask	✓		75.46	76.60	68.59
(e)	2D Mask	✓	✓	<b>80.73</b>	<b>81.70</b>	<b>73.61</b>

**a) Yaw estimation:** In table II we evaluate our approach for estimating camera viewpoint proposed in section III-C. First we experiment with a network  $\Phi$  tasked to output a vector  $\mathbf{x} \in \mathbb{R}^2$  with the yaw angle computed as  $\theta =$

$\arctan(x_1/x_2)$  (row (a)). Our direct prediction approach (rows (d-g)) outperforms this naïve baseline by a significant margin. Our method is influenced by the number of discrete rotations, 64 being optimal (row (f)). In order to provide stronger baselines, we additionally implement two alternative techniques [10], [8] to handle ambiguous predictions in 3D pose estimation, but did not observe a benefit (rows (b) and (c)) compared to simple direct arctan regression. This is perhaps due to the different setting ([10], [8] were proposed to handle ambiguous fitting of 3D shapes to 2D silhouettes).

TABLE II: Comparison of yaw prediction techniques.

Paradigm		AP <sub>BEV</sub> (IoU = 0.5)		
		Easy	Moderate	Hard
(a)	arctan	76.65	79.05	69.33
(b)	Insafutdinov & Dosovitskiy [10]	77.28	76.92	69.12
(c)	Goel et al. [8]	76.49	77.35	69.69
(d)	Ours, 16 bins	77.04	77.30	69.49
(e)	Ours, 32 bins	79.93	81.14	73.15
(f)	Ours, 64 bins	<b>80.73</b>	<b>81.70</b>	<b>73.61</b>
(g)	Ours, 128 bins	81.79	82.23	74.11

**b) SoTA comparison:** In table III we compare our method to the relevant state of the art. VS3D [29] uses a viewpoint estimation network pretrained on Pascal 3D and NYC 3D cars [42], [18] with ground truth yaw annotations. In Zakharov et al. [45] a synthetic dataset is used to initialise a coordinate shape space NOCS [38] providing a strong prior on 3D shape and yaw estimation. During fitting stage they only utilise Mask R-CNN predictions which have a high IOU compared to a ground truth 2D box and also takes 6 seconds to infer a single car on a modern GPU making it infeasible for real time prediction unlike VS3D [29] (22Hz) and our method which runs at 200Hz after the 2D object detection method (about 25Hz). We provide results (c) with a 2D detector trained on MS-COCO[16] for fairest comparison to this method which has pretrained requirements closest to our own. Frustum PointNet [27] is a fully supervised (2D box, yaw, 3D size, 3D centre) method trained on KITTI that serves as a reference with similar architecture to our method.

**c) Auto-Label Generation:** In table IV we compare different supervision options on a single model. We train the FPN [27] using original 3D ground truth, as well as only the 3D ground truth where there is a matching 2D detection from Mask-RCNN [40] (the same detector used in our method) to demonstrate what is the impact of instances missed by the 2D detector to the overall performance. We

TABLE III: Object Detection Average-Precision on the KITTI validation set. Compared to our Method VS3D[29] uses a network trained on Pascal 3D and NYC 3D Cars[42], [18] to determine the object Yaw and 2D box, while while Zakharov[44] only considers MASK R-CNN detections with an IOU > 50% compared to a ground truth box and uses a synthetic dataset to train a network which gives yaw.

Method	Annotations Source			AP <sub>BEV</sub> / AP <sub>3D</sub> (IoU = 0.5)		
	2D Boxes	3D		Easy	Moderate	Hard
		Yaw	Boxes			
(a) VS3D [29]	Pascal 3D	NYC Cars		74.5/40.32	66.71/37.36	57.55/31.09
(b) Zakharov et al. [44]	KITTI	KITTI		77.84/62.25	59.75/42.23	-/-
(c) <b>Ours</b>	MS-COCO			80.73/76.73	81.70/76.66	73.61/69.01
(d) <b>Ours</b>	Cityscapes			<b>86.52/83.45</b>	<b>86.22/79.53</b>	<b>75.53/71.01</b>
(e) <i>Frus.PointNet</i> [27]	KITTI	KITTI	KITTI	98.16/97.67	94.80/93.81	87.11/86.14

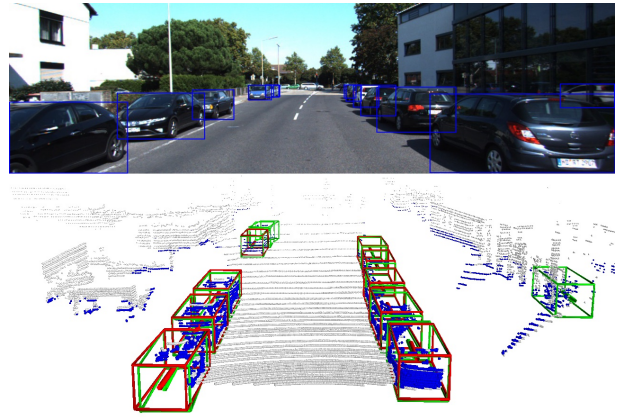


Fig. 6: Qualitative results of our method (green) on the KITTI Validation Set with ground truth car annotations in red and points inside each mask in blue.

show that the difference between our labelling method, which does not use any 3D ground truth, and using full 3D ground truth of only the instances that are “made available” by the 2D detector, is relatively small, and therefore the 2D detection quality is the main limiting factor.

TABLE IV: Using different forms of supervision to train Frustum PointNet [27]

Supervision	AP <sub>BEV</sub> (IoU = 0.5)		
	Easy	Moderate	Hard
Fully Supervised (original GT)	98.16	94.80	87.11
Fully Supervised (GT w/ matching dets.)	91.83	87.16	78.29
<i>Supervised by our labels (no GT)</i>	90.23	85.74	76.84

## V. CONCLUSIONS

In this paper we presented a novel method of localising 3D objects in LiDAR point clouds, trained using only generic 2D object detector. Compared to previous work, our method is less complex, we do not require the use of additional manually annotated data sources as in [29] or virtual data and ground truth 2D bounding boxes as in [45], and we still achieve superior accuracy and better run time. To our knowledge, our method is the first method that can learn to transform 2D predictions to 3D detections without any need for supervision of 3D parameters.

## ACKNOWLEDGEMENT

We are very grateful to Continental Corporation for sponsoring this research. Lukas was supported by OP VVV funded project CZ.02.1.01/0.0/0.0/16019/0000765 “Research Center for Informatics”.

## REFERENCES

- [1] Lucas Beyer, Alexander Hermans, and Bastian Leibe. Biternion nets: Continuous head pose regression from discrete training labels. In *German Conference on Pattern Recognition*, pages 157–168. Springer, 2015.
- [2] Holger Caesar, Varun Bankiti, Alex H. Lang, Sourabh Vora, Venice Erin Liong, Qiang Xu, Anush Krishnan, Yu Pan, Giancarlo Baldan, and Oscar Beijbom. nuscenes: A multimodal dataset for autonomous driving. *arXiv preprint arXiv:1903.11027*, 2019.
- [3] Xiaozhi Chen, Huimin Ma, Ji Wan, Bo Li, and Tian Xia. Multi-view 3d object detection network for autonomous driving. In *Proceedings of the IEEE conference on Computer Vision and Pattern Recognition*, pages 1907–1915, 2017.
- [4] Martin Engelcke, Dushyant Rao, Dominic Zeng Wang, Chi Hay Tong, and Ingmar Posner. Vote3deep: Fast object detection in 3d point clouds using efficient convolutional neural networks. In *2017 IEEE International Conference on Robotics and Automation (ICRA)*, pages 1355–1361. IEEE, 2017.
- [5] Di Feng, Lars Rosenbaum, Fabian Timm, and Klaus Dietmayer. Labels Are Not Perfect: Improving Probabilistic Object Detection via Label Uncertainty. *arXiv e-prints*, page arXiv:2008.04168, August 2020.
- [6] Huan Fu, Mingming Gong, Chaohui Wang, Kayhan Batmanghelich, and Dacheng Tao. Deep ordinal regression network for monocular depth estimation. In *CVPR*, June 2018.
- [7] Andreas Geiger, Philip Lenz, and Raquel Urtasun. Are we ready for autonomous driving? the KITTI vision benchmark suite. In *Conference on Computer Vision and Pattern Recognition (CVPR)*, 2012.
- [8] Shubham Goel, Angjoo Kanazawa, and Jitendra Malik. Shape and viewpoint without keypoints. In *Proc. ECCV*, 2020.
- [9] Kaiming He, Georgia Gkioxari, Piotr Dollár, and Ross B. Girshick. Mask R-CNN. In *Proc. ICCV*, 2017.
- [10] Eldar Insafutdinov and Alexey Dosovitskiy. Unsupervised learning of shape and pose with differentiable point clouds. In S. Bengio, H. Wallach, H. Larochelle, K. Grauman, N. Cesa-Bianchi, and R. Garnett, editors, *Advances in Neural Information Processing Systems 31 (NeurIPS 2018)*, pages 2804–2814, Montréal, Canada, 2018. Curran Associates.
- [11] Alex Kendall and Yarin Gal. What uncertainties do we need in Bayesian deep learning for computer vision? *Proc. NeurIPS*, 2017.
- [12] Alex Kendall, Matthew Grimes, and Roberto Cipolla. PoseNet: A convolutional network for real-time 6-DOF camera relocation. In *Proceedings of the IEEE international conference on computer vision*, pages 2938–2946, 2015.
- [13] L. Koestler, N. Yang, R. Wang, and D. Cremers. Learning monocular 3d vehicle detection without 3d bounding box labels. In *Proceedings of the German Conference on Pattern Recognition (GCPR)*, 2020.
- [14] Shuai Liao, Efstratios Gavves, and Cees GM Snoek. Spherical regression: Learning viewpoints, surface normals and 3d rotations on n-Spheres. In *Proceedings of the IEEE/CVF Conference on Computer Vision and Pattern Recognition*, pages 9759–9767, 2019.
- [15] Tsung-Yi Lin, Michael Maire, Serge Belongie, James Hays, Pietro Perona, Deva Ramanan, Piotr Dollár, and C Lawrence Zitnick. Microsoft coco: Common objects in context. In *European conference on computer vision*, pages 740–755. Springer, 2014.
- [16] Tsung-Yi Lin, Michael Maire, Serge J. Belongie, James Hays, Pietro Perona, Deva Ramanan, Piotr Dollár, and C. Lawrence Zitnick. Microsoft COCO: common objects in context. In *Proc. ECCV*, 2014.
- [17] Francisco Massa, Renaud Marlet, and Mathieu Aubry. Crafting a multi-task CNN for viewpoint estimation. *arXiv preprint arXiv:1609.03894*, 2016.
- [18] Kevin Matzen and Noah Snavely. Nyc3dcars: A dataset of 3d vehicles in geographic context. In *Proc. Int. Conf. on Computer Vision*, 2013.
- [19] Qinghao Meng, Wenguan Wang, Tianfei Zhou, Jianbing Shen, Luc Van Gool, and Dengxin Dai. Weakly supervised 3D object detection from LiDAR point cloud. In *ECCV*, 2020.
- [20] Arsalan Mousavian, Dragomir Anguelov, John Flynn, and Jana Kosecka. 3D bounding box estimation using deep learning and geometry. In *Proceedings of the IEEE Conference on Computer Vision and Pattern Recognition*, pages 7074–7082, 2017.
- [21] David Novotný, Diane Larlus, and Andrea Vedaldi. Learning 3D object categories by looking around them. In *Proceedings of the International Conference on Computer Vision (ICCV)*, 2017.
- [22] Jeong Joon Park, Peter Florence, Julian Straub, Richard Newcombe, and Steven Lovegrove. DeepSDF: Learning continuous signed distance functions for shape representation. In *The IEEE Conference on Computer Vision and Pattern Recognition (CVPR)*, June 2019.
- [23] Adam Paszke, Sam Gross, Francisco Massa, Adam Lerer, James Bradbury, Gregory Chanan, Trevor Killeen, Zeming Lin, Natalia Gimelshein, Luca Antiga, Alban Desmaison, Andreas Kopf, Edward Yang, Zachary DeVito, Martin Raison, Alykhan Tejani, Sasank Chilamkurthy, Benoit Steiner, Lu Fang, Junjie Bai, and Soumith Chintala. Pytorch: An imperative style, high-performance deep learning library. In H. Wallach, H. Larochelle, A. Beygelzimer, F. d’Alché-Buc, E. Fox, and R. Garnett, editors, *Advances in Neural Information Processing Systems 32*, pages 8024–8035. Curran Associates, Inc., 2019.
- [24] Hugo Penedones, Ronan Collobert, Francois Fleuret, and David Grangier. Improving object classification using pose information. Technical report, Idiap, 2012.
- [25] Bojan Pepik, Michael Stark, Peter V. Gehler, and Bernt Schiele. Teaching 3D geometry to deformable part models. In *Proc. CVPR*, 2012.
- [26] Sergey Prokudin, Peter Gehler, and Sebastian Nowozin. Deep directional statistics: Pose estimation with uncertainty quantification. In *Proceedings of the European Conference on Computer Vision (ECCV)*, pages 534–551, 2018.
- [27] Charles R Qi, Wei Liu, Chenxia Wu, Hao Su, and Leonidas J Guibas. Frustum pointnets for 3d object detection from rgb-d data. *arXiv preprint arXiv:1711.08488*, 2017.
- [28] Charles R. Qi, Hao Su, Kaichun Mo, and Leonidas J. Guibas. PointNet: Deep learning on point sets for 3D classification and segmentation. *arXiv preprint arXiv:1612.00593*, 2016.
- [29] Zengyi Qin, Jinglu Wang, and Yan Lu. Weakly supervised 3D object detection from point clouds. In *Proc. ACMM*, 2020.
- [30] Shaoqing Ren, Kaiming He, Ross B. Girshick, and Jian Sun. Faster R-CNN: towards real-time object detection with region proposal networks. In *Proc. NeurIPS*, 2016.
- [31] Ashutosh Saxena, Justin Driemeyer, and Andrew Y Ng. Learning 3-d object orientation from images. In *2009 IEEE International conference on robotics and automation*, pages 794–800. IEEE, 2009.
- [32] S. Song, S. P. Lichtenberg, and J. Xiao. Sun rgb-d: A rgb-d scene understanding benchmark suite. In *2015 IEEE Conference on Computer Vision and Pattern Recognition (CVPR)*, pages 567–576, 2015.
- [33] Hao Su, Charles R Qi, Yangyan Li, and Leonidas J Guibas. Render for CNN: Viewpoint estimation in images using CNNs trained with rendered 3D model views. In *Proceedings of the IEEE International Conference on Computer Vision*, pages 2686–2694, 2015.
- [34] Pei Sun, Henrik Kretzschmar, Xerxes Dotiwalla, Aurelien Chouard, Vijaysai Patnaik, Paul Tsui, James Guo, Yin Zhou, Yuning Chai, Benjamin Caine, et al. Scalability in perception for autonomous driving: Waymo open dataset. In *Proceedings of the IEEE/CVF Conference on Computer Vision and Pattern Recognition*, pages 2446–2454, 2020.
- [35] Shubham Tulsiani, Alexei A Efros, and Jitendra Malik. Multi-view consistency as supervisory signal for learning shape and pose prediction. In *Proceedings of the IEEE conference on computer vision and pattern recognition*, pages 2897–2905, 2018.
- [36] Shubham Tulsiani and Jitendra Malik. Viewpoints and keypoints. In *Proc. CVPR*, 2015.
- [37] Dominic Zeng Wang and Ingmar Posner. Voting for voting in online point cloud object detection. In *Robotics: Science and Systems*, volume 1, pages 10–15607. Rome, Italy, 2015.
- [38] He Wang, Srinath Sridhar, Jingwei Huang, Julien Valentin, Shuran Song, and Leonidas J. Guibas. Normalized object coordinate space for category-level 6d object pose and size estimation. In *The IEEE Conference on Computer Vision and Pattern Recognition (CVPR)*, June 2019.
- [39] Peng Wang, Xinyu Huang, Xinjing Cheng, Dingfu Zhou, Qichuan Geng, and Ruigang Yang. The apolloscape open dataset for autonomous driving and its application. *IEEE transactions on pattern analysis and machine intelligence*, 2019.
- [40] Yuxin Wu, Alexander Kirillov, Francisco Massa, Wan-Yen Lo, and Ross Girshick. Detectron2. <https://github.com/facebookresearch/detectron2>, 2019.
- [41] Yu Xiang, Roozbeh Mottaghi, and Silvio Savarese. Beyond PASCAL: A benchmark for 3D object detection in the wild. In *Proc. WACV*, 2014.
- [42] Yu Xiang, Roozbeh Mottaghi, and Silvio Savarese. Beyond pascal: A benchmark for 3d object detection in the wild. In *IEEE Winter Conference on Applications of Computer Vision (WACV)*, 2014.

- [43] Yu Xiang, Tanner Schmidt, Venkatraman Narayanan, and Dieter Fox. Posecnn: A convolutional neural network for 6d object pose estimation in cluttered scenes. *arXiv preprint arXiv:1711.00199*, 2017.
- [44] Sergey Zakharov, Wadim Kehl, Arjun Bhargava, and Adrien Gaidon. Autolabeling 3D objects with differentiable rendering of SDF shape priors. In *IEEE Computer Vision and Pattern Recognition (CVPR)*, June 2020.
- [45] Sergey Zakharov, Wadim Kehl, Arjun Bhargava, and Adrien Gaidon. Autolabeling 3D objects with differentiable rendering of SDF shape priors. In *Proc. CVPR*, 2020.
- [46] Yin Zhou and Oncel Tuzel. Voxelnet: End-to-end learning for point cloud based 3d object detection. In *Proceedings of the IEEE Conference on Computer Vision and Pattern Recognition*, pages 4490–4499, 2018.